Solar Power System Analyses for Electric Propulsion Missions

Thomas W. Kerslake and Leon P. Gefert
Glenn Research Center, Cleveland, Ohio

National Aeronautics and
Space Administration

Glenn Research Center

July 1999

This report contains preliminary findings, subject to revision as analysis proceeds.

Solar Power System Analyses for Electric Propulsion Missions

Thomas W. Kerslake and Leon P. Gefert
National Aeronautics and Space Administration
Glenn Research Center
Cleveland, Ohio 44135

ABSTRACT

Solar electric propulsion (SEP) mission architectures are applicable to a wide range of NASA missions including human Mars exploration and robotic exploration of the outer planets. In this paper, we discuss the conceptual design and detailed performance analysis of an SEP stage electric power system (EPS). EPS performance, mass and area predictions are compared for several PV array technologies. Based on these studies, an EPS design for a 1-MW class, Human Mars Mission SEP stage was developed with a reasonable mass, 9.4 metric tons, and feasible deployed array area, 5800 m2. An EPS was also designed for the Europa Mapper spacecraft and had a mass of 151 kg and a deployed array area of 106 m2.

INTRODUCTION

Traditionally, electric propulsion has been proposed for interplanetary missions since it affords very mass efficient exploration architectures [1,2]. However, to obtain reasonable transfer times, very large power levels (multi-MW class) were required. Power requirements drop dramatically to the 0.5 to 1.0 MW when aerobrake and cryogenic upper stage transportation technologies are utilized with electric propulsion. For ~1 MW power levels, solar photovoltaic (PV) systems are an attractive alternative to nuclear dynamic systems to satisfy power requirements.

In this architecture, the efficient solar electric propulsion (SEP) stage transfers the payload from low Earth orbit (LEO) to a High Energy Elliptical Parking Orbit (HEEPO). A high-thrust, cryogenic upper stage then injects the payload to it's planetary target allowing for fast heliocentric trip times. This mission architecture, shown in Figure 1 for a human Mars mission, offers a potential reduction in mass to LEO compared to alternative all-chemical or nuclear propulsion schemes. Such a Mars mission could take place in the 2010-2020 time frame. LEO mass savings can also be realized for outer planetary missions, such as the Europa Mapper Mission. Mass reductions may allow launch vehicle down-sizing and enable missions that would have been grounded due to cost constraints.

Figure 2 illustrates a conceptual SEP stage design for a human Mars mission [3]. This stage has a dry mass of 35 metric tons (MT), 40 MT of xenon propellant and a 5800 m2 PV array that spans ~110-m providing power to a cluster of eight, 100-kW, Hall thrusters. This stage can transfer an 80 MT payload and upper stage to the desired HEEPO. By comparison, the 1980's technology international space station, when completed, will have a mass of 450 MT, a span of 110-m, 2500 m2 of array area and 0.24 MW of daytime PV array power (US PV arrays only). As another comparison, the SEP PV array segments have dimensions about twice those of the next generation space telescope sun shield currently under development. Preliminary packaging studies have been performed to integrate the SEP stage with the proposed "Magnum" launch vehicle [4]. These studies showed the stowed SEP stage can meet Magnum mass and volume requirements with considerable margin.

In this paper, we discuss the conceptual design and analysis for the SEP stage electric power system (EPS). EPS performance, mass and area predictions are compared for several PV array technologies.

MISSION TRAJECTORY ANALYSIS

HUMAN MARS MISSION

The SEP stage is first used for transfer from a 51.6° inclination, 400-km circular LEO to a 800 x 65,000 km HEEPO. This transfer can take 6-12 months depending on the SEP system size and total initial mass in LEO. In HEEPO, the SEP stage separates from the Mars payload and cryogenic stage combination. The SEP stage then returns to LEO for reuse. The cryogenic stage injects the payload from HEEPO to an Earth-Mars transfer trajectory. The empty cryogenic stage then separates from the payload. The payload captures into Mars orbit using an aerocapture system.

Each thruster operates with a specific impulse range of 2000 to 3000 sec, a combined thruster plus power conditioning efficiency of 64% and a thrust of 6 Newtons. At these low thrust levels, orbit transfers cannot be approximated with impulsive maneuvers. A low-thrust level orbit transfer must be approximated by the explicit integration of all forces acting on the vehicle, including the thrusters. For these analyses, a high fidelity trajectory integration program was used in conjunction with an innovative, four-phased analytic steering law [3]. The primary goal was to target different final HEEPOs while minimizing propellant use for fixed time transfers.

A secondary goal was to minimize time spent in the Earth's proton radiation belts (primary contributor to PV cell degradation).

EUROPA MAPPER

The SEP mission architecture for Jovian planetary missions and Mars missions are similar in the early mission phase, i.e. LEO to HEEPO. Thereafter, the Jovian mission architecture differs. The SEP vehicle is not staged but instead injected with the payload into a 2-year, elliptical Earth orbit. An Earth gravity assist maneuver is then used to inject the spacecraft on a Jovian trajectory. Minor delta-velocity maneuvers are performed by the SEP stage prior to ejecting the electric propulsion system hardware. However, the SEP EPS remains as the spacecraft power source. And finally, a different "end game" strategy is employed. This strategy may include aerobraking, aerocapture, chemical propulsive capture and/or gravity assist "pump down" to achieve the final desired mapping orbit around Europa. The other important difference is the physical size and power requirements of the Europa SEP stage is dramatically smaller than a human Mars mission SEP stage, i.e. 15 kW, compared to 1 MW.

EPS DESIGN

The EPS employs a channelized, 500-Vdc, power management and distribution (PMAD) architecture featuring 16 channels feeding eight 100-kWe thrusters (see Figure 3). Each channel includes a PV section, a solar fine-pointing gimbal and an array regulator unit (ARU) that feeds a central power distribution unit (PDU) via power distribution cabling. Since the SEP stage operates in a solar inertial attitude, no solar tracking gimbal is required for planar PV arrays. However, for linear concentrator PV arrays, tracking gimbals are required to maintain primary axis Sun tracking within 2°. Gimbal performance characteristics were derived by scaling those of the International Space Station (ISS) PV Module beta gimbal design.

The PDU distributes power from PV array sections to the thruster power processing units (PPUs). The PDU contains stage/payload power supplies, charge/discharge equipment for the lithium ion batteries, PV array deployment controller and microcomputer. Since the thrusters do not operate in eclipse periods, the batteries store only a modest amount of energy (about 13 kW-hr) needed for payload and SEP stage housekeeping loads. The PDU and batteries are actively cooled by a pumped fluid loop thermal control system (TCS) with deployable aluminum honeycomb radiator panels and a pump/flow-control unit.

The 500-V PMAD voltage was selected for several reasons. It permits "direct drive" thruster operation that greatly reduces the PPU size, complexity and power loss [5]. The high voltage level reduces conductor current density allowing use of smaller gage, less massive conductors. Yet the voltage level is low enough to still allow use of standard mil-spec aerospace power cabling. Paralleled, gage 0 copper conductors with Teflon type insulation were selected to satisfy bundle derated current limits and provide some redundancy. Space plasma effects data (arcing and parasitic leakage current) were measured during the PASP PLUS mission for several PV cell types biased up to +/- 500-V with respect to the plasma [6]. Similar tests were performed on the Shuttle-based SAMPIE flight experiment [7]. And lastly, 600-V silicon and silicon-carbide based technology development is well underway at NASA for switch gear components and remote power controllers [8].

Several PV array designs and PV cell technologies were considered: (1) the ISS PV array design with 8x8 cm, crystalline silicon PV cells (as a baseline), (2) a linear concentrator array, based on the SCARLET array design [9], employing 2x8 cm crystalline, 3-junction GaInP2/GaAs/Ge cells operating at 7.5x solar concentration, (3) thin film, 3-junction, 5x5 cm amorphous silicon-germanium (a-SiGe) cells [10] on folded thin (2-mil) polymer membranes and (4) 5x5 cm, CuInS2 thin film cells [11-13] on thin (2-mil) polymer membranes. The thin film cells are encapsulated with 1.5-mil thick FEP Teflon for isolation from the space plasma. PV array membranes are deployed using an inflatable (rigidized) longitudinal column and a flexible composite lateral member (Figure 2). This design concept is based on that proposed for the Next Generation Space Telescope Sun shield [14,15]. Column and member properties were selected to satisfy buckling and squirming instability requirements. Properties were also chosen to ensure sufficient membrane tension (to remove membrane wrinkles and maintain membrane flatness) during thermal deformations associated with orbital sun-shade cycles.

The PV array was divided into 16 independent electrical sections each rated at approximately 50 kW. Array strings were negative grounded and contained a sufficient number of series-connected cells to provide 500* volts maximum power voltage at end-of-life. A by-pass diode was incorporated for every 10 cells to reduce array long-term degradation. The number of parallel strings was selected to meet power requirements. PV array designs incorporate a flat copper multi-ribbon power harness encapsulated in polyimide. Conductor cross section was sized to provide a 3% $\Delta V/V$. PV array surfaces are coated with a transparent conducting metal oxide, such as indium tin oxide, to prevent space charge buildup and arcing at high orbit altitudes.

Similar EPS architecture, designs and technology were assumed for the Europa Mapper spacecraft. The

primary exception was that the PV array was assumed to consist of two, rectangular wings, each rated to deliver approximately 7.5 kW in Earth orbit.

EPS MASS ESTIMATES

PV array mass estimates for the ISS and SCARLET type designs were based on as-built panel masses, 2.4 kg/m2 and 3.8 kg/m2, respectively, plus 20% extra mass for launch containment and deployment structures. For thin membrane arrays, the membrane areal mass was calculated based on specified layer thicknesses and material densities. This mass calculation included encapsulant, adhesive, cell contacts and interconnects, and substrate. Launch containment structures, deployed structures and inflation/rigidization equipment was assumed twice as massive as the ~0.2 kg/m2 membrane mass. The power harness mass was based on that for the ISS PV array and scaled by conductor current level.

Gimbal mass (1.4 kg/kW) and ARU mass (2.5 kg/kW) were scaled from the ISS beta gimbal and sequential shunt unit masses, respectively. The PDU mass, 0.3 kg/kW, was calculated assuming PEBB-based, year 2005 technology components. Lithium ion battery mass was assumed to be 12.5 kg/kW-hr. The TCS mass, 0.4 kg/kWe (transferred through the PDU), was based on the ISS PV module TCS system. Power cabling mass was calculated based on run length, number of conductors, insulation type and Mil-W-22759D conductor mass properties.

PPU mass was not book kept as part of the EPS mass budget. Also, component heaters and associated wiring masses were not estimated. Margins were not applied to the mass estimates.

EPS PERFORMANCE ANALYSIS

POWER REQUIREMENTS

For the human Mars mission architecture, the EPS was designed to provide a high power level to the Hall thruster PPUs during orbital insolation and a low power level to the payload continuously through the mission for two successive LEO-to-HEEPO transits. Two payloads are delivered to HEEPO by the first transfer and one payload is delivered to HEEPO by the second transfer. During the first transfer, the EPS was required to deliver 800-kW at 500-V to the input of the Hall thruster PPUs. This requirement decreased to 750-kW for the second transfer. The payload and SEP housekeeping continuous power requirement was 13 kW.

For the Europa Mapper spacecraft, the power requirement was 15 kW at 500-V to the PPU input while in Earth orbit (at 1 AU). A second requirement was to provide 200 W of power to spacecraft payloads and housekeeping loads while in Europa orbit.

COMPUTATIONAL METHODS

A dedicated Fortran computer code was written to analyze EPS performance and calculate EPS mass. The code runs on a SGI Indigo 2 work station. Most computational methods employed were borrowed from the EPS analysis code SPACE [16] developed by NASA for the ISS program. Nested iteration loops solve for PV array current, voltage and temperature in addition to PMAD system currents and voltages. Based on an analysis time step sensitivity study, a 30-minute time step was selected. This value provided a reasonable balance of solution accuracy/resolution and computer file size / run time for 1200-day mission analysis runs.

ENVIRONMENTS

Several orbital environments are important to high-voltage operation of PV power systems in Earth orbit. These environments were modeled within the Fortran computer codes and were evaluated throughout the mission analysis. Environmental models included: thermal, particulate radiation, meteoroid/debris and plasma. The thermal model calculated incident PV array heat fluxes from the Sun, Earth albedo and Earth infrared radiation [17,18]. Proton and electron fluences were calculated using the AP8MIN/MAX and AE8MIN/MAX models [19,20]. Damage equivalent normally incident (DENI) 1-MeV electron fluence [21] was then determined using calculated effective shielding values and damage coefficients from [22]. Meteoroid/debris fluences were calculated from [23-25] while incipient penetration and cratering area ratios were from [26,27]. Damage from secondary ejecta impacts was not modeled. Plasma characteristics were from [28,29]. PV array degradation factors from other important environmental effects, such as contamination, ultraviolet (UV) radiation and thermal cycling, were incorporated via data input files.

Additional environments important for PV power system operation on the Europa Mapper spacecraft include solar flare radiation events (assumed at 2 per year) [30], meteoroids, asteroids (not modeled), Jupiter and Europa radiation belts (not modeled) and Jupiter ring debris (not modeled). Galactic cosmic radiation damage was ignored due to the negligible total dose accumulated by solar cells.

PHOTOVOLTAIC ARRAYS

PV array thermal-electrical performance was evaluated throughout the mission. Starting at the solar cell level, current-voltage (IV) response was modeled by a single exponential relationship based on four cell parameters (short-circuit current, open-circuit voltage and maximum

power current and voltage). These cell parameters were corrected for temperature and environmental factors. Cell thermal response was based on a transient, lumped-parameter energy balance model. Cell operating IV point and temperature were iteratively determined. The solar cell string IV curve was determined by voltage addition of series-connected cells and accounting for the resistance of cell interconnects and power harness conductors. Correction factors were applied for solar insolation intensity, cell mismatch, array flatness and solar pointing error. PV array section total current was then determined by summing the parallel-connected string currents. Total PV array area was determined by the total cell area divided by the cell areal packing density (0.64, 0.85 and 0.90 for ISS, concentrator and thin film PV array types, respectively).

Cell IV parameters, temperature coefficients, optical properties, UV metastability (Staebler-Wronski effect in a-Si cells only), radiation degradation, and thermal cycling degradation were obtained from and/or scaled from the following sources: ISS silicon cells [31,32], GaInP2/GaAs/Ge cells [9,33], a-SiGe cells [10,34,35] and CuInS2 cells [11,12]. UV and particle radiation darkening of coverslides, adhesives, refractive lens and polymeric encapsulants [36] and substrates was implemented as time-dependent changes in solar absorptance, transmittance and thermal emittance. Non-volatile contaminant losses were treated in the same manner while assuming the same contaminant species as for ISS PV arrays, but only 50% of the deposition rate [37]. Particulate contamination losses were assumed to be small and thus, ignored. Plasma leakage current was calculated as the product of the PV array frontal area and the electron thermal current density, Je, assuming the high-voltage array operates in a "snap-over" condition (i.e., capacitively coupled insulator surfaces collect electrons) [38]. For a planar surface, Je is given by:

$$Je = (Ne^*e/4) * [8^*k^*Te / (\pi^* m)]^{**}0.5 , \qquad (1)$$

where e is the electron unit charge, m is the electron mass, k is the Boltzmann constant and Ne and Te are the orbit altitude-dependent electron number density and temperature, respectively [38]. A correction factor, 0.01, was applied to the calculated leakage current values for the concentrator array to reflect the influence of design geometry and materials as measured by [6].

ENERGY STORAGE

Because of the relatively small EPS mass and performance impacts of the energy storage subsystem, lithium ion battery IV characteristics were not modeled. Instead the maximum energy storage value was calculated and the battery mass estimated as described above.

POWER MANAGEMENT & DISTRIBUTION

The PV array gimbals (if present), ARU and PDU were electrically modeled as resistive and diode voltage drops based on ISS PMAD components. Power cable voltage drops were calculated based on specified resistance, operating temperature and run lengths. The small resistance of connectors was assumed to be accounted for in PMAD component resistances.

THERMAL CONTROL

In addition to PVA temperatures, PMAD component temperatures were also calculated based on a transient, lump-capacitance modeling. The PV array gimbal was assumed to be cylindrical while all other components were assumed to be rectangular. For rectangular components, the mounting face was assumed adiabatic while another face was assumed to be fixed normal to the Sun vector. The component energy balance included terms from solar flux, Earth albedo, Earth infrared heat flux and internal heat dissipation, heater power or active cooling. Component masses and volumes were scaled from similar ISS components. Component optical properties were assumed consistent with either anodized aluminum or Z-93 white painted surfaces and were selected for temperature range control. High and low end temperature limits were specified for each component based on ISS hardware or state-of-the-art technology values when available.

Thermal control cooling load was calculated for the PDU and batteries and electric heater power load was calculated for all components. Cooling and heating loads were calculated such that minimum or maximum component temperatures were maintained.

RESULTS

HUMAN MARS MISSION

EPS mass and array area values are shown in Table 1 for four PV array technologies. The results show that EPS mass and size are dominated by the PV array. Moreover, the long transit times in the Earth proton belts cause tremendous power degradation. This is indicated by the high BOL power levels required to deliver 813 kW and 763 kW during the transfer to HEEPO. Because of the high degradation, non-radiation hardened PV array designs, i.e. ISS, must be over sized so much that the EPS mass (46 MT) and deployed area (13,984 m2) become unwieldy. Even when the ISS cell coverglass thickness, 5-mil, was double or tripled, marginal performance gains were realized. The smallest array size, 3472 m2, was provided by the high-efficiency, radiation-hard, concentrator array. But this array design is massive (16 MT) due to the honeycomb panel construction and lens support structures employed. In

the years following SCARLET design completion, several alternative design options have been proposed that could significantly reduce the mass a concentrator array [39]. Clearly, the lightest EPS options (9-12 MT range) employ thin panel PV arrays. However, thin panel arrays require significant deployed areas (6000-9000 m2 range) due to their relatively low conversion efficiencies. Of the thin film cell options, the CuInS2 cells provides superior projected performance and no Staebler-Wronski losses which allows for the smallest feasible PV array size. However, the CuInS2 cell design and manufacturing maturity is lower than the competing a-SiGe cell technology that has a strong terrestrial manufacturing base [40].

Current, voltage and power at the PPU input for the a-SiGe array option is shown in Figure 4. Power falls rapidly during the first 200-days as the SEP stage spirals through the proton belts and sustains the bulk of the mission radiation damage. Once the vehicle apogee is above ~4 Earth radii, little addition degradation is incurred. From 400 to 800 days, a 1100 km parking orbit is maintained to await the next payload transfer opportunity. This orbit is below the main proton belt and thus, little radiation dose is accumulated during this time period. During the second LEO to HEEPO transfer, power degrades somewhat more but the 763 kW power requirement is met.

PV array current and voltage degradation factors are shown in Figures 5a and 5b, respectively, for the a-SiGe array. The largest contributor to degradation is radiation damage followed by Staebler-Wronski loss and then encapsulant transmission loss. The sinusoidal variation in the current loss factor (Figure 5a) reflects the yearly change in solar insolation. The dispersion in voltage loss factor from 400 to 800 days (Figure 5b) reflects the impact of different cell temperature data points corresponding to different positions within the orbit Sun or eclipse periods.

Figure 6 shows the DENI fluence, given in electrons/cm2, predicted for the a-SiGe array option. Cell voltage, with a 1.3E15 fluence, is more sensitive to the radiation environment than is cell current, with a fluence of 5.9E14.

Figure 7 shows the plasma parasitic leakage current for the ISS cell technology. Early in the mission, the SEP stage altitude is low and electron densities are high. As such, the ISS type array collects over 250 amps during short periods of time. To maintain SEP stage potential near that of the plasma, excess electrons must be rejected. This is accomplished by operating the thruster cathode at a higher current than is necessary for beam neutralization. During eclipse periods when the thrusters are not operating, the array voltage is negligible and

electrons are not collected. If the SEP stage is in sunlight with the thrusters not operating, most of the arrays strings will be shunted to manage power production as well as manage stage floating potential. Based on flight test data and the relatively small deployed area, the concentrator array has very small parasitic leakage current. The thin film arrays are assumed to be perfectly insulated and grounded. Under theses assumptions, no electrons will be collected. As the mission proceeds, however, high voltage cells and conductors will be exposed to the plasma as the result of impact craters, delamination, etc. Under this scenario, the electron current collection is still negligible based on the calculated area exposed and plasma sheath geometry.

PV array temperature is shown in Figure 8 for the a-SiGe array. Throughout most of the mission, the array operates in the 50°C to 75°C temperature range. Occasionally, very cold temperatures, i.e. -155°C, are predicted during eclipse periods at moderately high apogees of 32,000 km.

PMAD component temperatures through the mission are shown in Figure 9. After appropriate selection of component surface optical properties, most components stayed within their allowable operating temperature range for most of the mission. Early in the mission, the PDU and batteries hit their upper operating temperature limits and active cooling is required. This cooling load reached a maximum of 22 kWt and then falls off to 0 kWt after ~130 days into the mission. Sporadically, the PDU reached it's lower temperature limit. Thus, heater power in the range of 100 to 200 W was required for a short time interval during some eclipse periods.

EUROPA MAPPER

Table 2 shows EPS mass, array area, power and temperatures for the Europa spacecraft at 1 AU and at 5.2 AU (Jovian orbit). At an EPS mass of only 151 kg, the thin film a-SiGe array option is clearly lighter than the concentrator array option for the same performance. This array would require two wings, each with a 53 m2 area. At Jupiter, with a -130°C array temperature, the EPS could provide about 400 W to spacecraft loads at the beginning of the end game. Allowing for a 50% loss in power due to radiation degradation during a 1-year pump down and a 1-year Europa mission, the 200 W power requirement could still be met assuming the arrays wings could track the Sun without large pointing loss.

CONCLUSIONS

Based on a conceptual design and detailed performance calculations, an EPS design for a Human Mars Mission

SEP stage was developed that fully met power requirements with reasonable mass, 9.4 MT, and feasible deployed array area, 5800 m2. The SEP architecture is also attractive for outer planetary missions. An EPS was designed to meet the 15 kW Hall thruster and 200 W Europa Mapper spacecraft power requirements at a mass of 151 kg and a total array deployed area of 106 m2.

CONTACT

Thomas W. Kerslake is an aerospace engineer in the Power & Propulsion Office. Phone 216-433-5373. Email kerslake@grc.nasa.gov

REFERENCES

1. Hack, K. J., et al., "Nuclear Electric Propulsion Mission Performance for Fast Piloted Mars Missions," AIAA Paper No. 91-3488, Sep 1991.

2. Hickman, J. M., et. al., "Solar Electric Propulsion for Mars Transport Vehicles," NASA Technical Paper 103224, Sep 1990.

3. Gefert, Leon P., et al., "Options for the Human Exploration of Mars using Solar Electric Propulsion," STAIF Conference, Albuquerque, New Mexico, Jan 1999.

4. Dudzinski, Leonard A., NASA Glenn Research Center, personal communication, 1998.

5. Hamley, John A., et al., "Hall Thruster Direct Drive Demonstration," paper AIAA97-2787, 33rd AIAA/ASME/SAE/ASEE Joint Propulsion Conference and Exhibit, Seattle Washington, Jul 6-9, 1997.

6. Guidice, D. A., et al., "Survey of Experimental Results From One Year of PASP PLUS Orbital Operation," AIAA 27th Plasmadynamics and Lasers Conference, Nov 14, 1996.

7. Ferguson, Dale C., and Hillard, G. Barry, "Preliminary results from the flight of the Solar Array Module Plasma Interactions Experiment (SAMPIE)," Proceedings of the 13th Space Photovoltaic Research and Technology Conference (SPRAT 13), Sep 01, 1994, p. 247-256 .

8. George, Patrick, "Space Solar Power Technology Plan FY 99: Power Management and Distribution," NASA Lewis Research Center, 1998.

9. Murphy, David M. and Allen, Douglas M., "SCARLET Development, Fabrication and Testing for the Deep Space 1 Spacecraft," 32nd Intersociety Energy Conversion Engineering Conference Proceedings, paper no. 97539, Aug 1997.

10. Jang, Jeffrey, et. al., "Recent Progress in Amorphous Silicon Alloy Leading to 13% Stable Cell Efficiency," 26th IEE PVSC, Anaheim, CA, Sep 29- Oct 3, 1997.

11. Bulent, M. Basol. et al., "Light-Weight, Flexible Thin Film Solar Cells for Space Applications," NASA CR 195466, Jun 1995.

12. Mitchell, K.W., et al., "7.3% Efficient CuInS2 Solar Cell," IEEE PVSE, 1988.

13. Landis, Geoffrey A., and Hepp, Aloysius F., "Applications of Thin-Film Photovoltaics for Space," 36th Intersociety Energy Conversion Engineering Conference, Aug 1991, p. 256-261.

14. http://www.ilcdover.com/AeroDef/Space/ngst.htm

15. http://ngst.gsfc.nasa.gov/Hardware/text/deploy.html

16. Hojnicki, J. S., et al., "Space Station Freedom Electrical Performance Model," 28th Intersociety Energy Conversion Engineering Conference Proceedings, Atlanta, Georgia, 1993.

17. Anon., "Space Station Program Natural Environment Definition for Design," SSP 30425 Rev. B, Nov 1993, pp. 10-5.

18. Farner, D. L., "The Effect of Diurnal Variation on Short Time Interval Averages of Albedo and Thermal Radiation," Lockheed TM LESC-30539, May 1993.

19. Sawyer, D. M. and Vette, J. I., " AP-8 trapped proton environment for solar maximum and solar minimum," NASA-TM-X-72605, Dec 01, 1976.

20. Jordan, Carolyn E., " NASA radiation belt models AP-8 and AE-8," Report AD-A223660, Sep 30, 1989.

21. Anspaugh, B. E., "GaAs Solar Cell Radiation Handbook," NASA-CR-203421, Jul 01, 1996.

22. Curtis, Henry B., NASA Glenn Research Center, personal communication, 1998.

23. Cour-Palais, B. G., "Meteoroid Environment Model -1969 (Near Earth to Lunar Surface)," NASA SP 8013, 1969.

24. Kessler, D. J., et al., "Orbital Debris Environment for Spacecraft Designed to Operate in Low Earth Orbit," NASA TM 100471, April 1989.

25. Kessler, D. J., et al., "A Computer-Based Orbital Debris Model for Spacecraft Designs and Observations in Low-Earth Orbit," NASA TM 104825, Nov 1, 1996.

26. Eichelberger, R. J., and Kineke, J. H., Jr., Hypervelocity Impact," SPRINGER-VERLAG, Jan 1, 1967, p. 659-692.

27. Myre, Craig A., "Hypervelocity Particle Impact Testing of Solar Array Coupons," Preliminary Information Report #259, NASA Lewis Research Center, May 30, 1991.

28. Anderson, B. Jeffrey and Smith, Robert E., "Natural orbital environment definition guidelines for use in aerospace vehicle development," NASA-TM-4527, Jun 01, 1994.

29. Smith, R. E. and West, G. S., "Space and planetary environment criteria guidelines for use in space vehicle development. Volume 1: 1982 revision," NASA-TM-82478, Jan 01, 1983.

30. Tada, H. Y. et al., "Solar Cell Radiation Handbook," NASA-CR-169662, Nov 01, 1982.

31. Bunyan, S. M., "Space Station Freedom Solar Cell Assembly Mini-Qualification Test Report," Engineering Report No. 210-906, Spectrolab Inc., Jun 27, 1996.

32. Scheiman, D. A. and Smith, B. K., "Rapid Thermal Cycling of Solar Array Blanket Coupons for Space Station Freedom," Solar Engineering, Vol 2., ASME, p. 817-823.

33. Eskenazi, Michael I., et al., "Balloon and Lear Jet Testing of SCARLET Modules and Cells," Proceedings of the 16th Space Photovoltaic Research and Technology Conference (SPRAT 16), 1997.

34. Boswell, J., et al., "Thin Film Photovoltaic Development at Phillips Laboratory," IEEE PVSC, 1993, p. 1324-1329.

35. Byvik, C. E., et al., "Radiation Damage and Annealing of Amorphous Silicon Solar Cells," IEEE PVSC, 1984.

36. Zuby, Thomas M., et al., "Degradation of FEP Thermal Control Materials Returns form the Hubble Space Telescope," NASA TM 104627, Dec 1995.

37. Anon., "Space Station External Contamination Control Requirements," SSP 30426 Rev. B, Jul 1991.

38. Ferguson, Dale C., NASA Glenn Research Center, personal communication, 1998.

39. Murphy, David M., AEC Able Engineering Inc., personal communication, 1998.

40. Guha, S., et. al., "Triple Junction Amorphous Silicon Alloy PV Manufacturing Plant if 5 MW Annual Capacity," 26th IEEE PVSC, Anaheim, CA, Sept. 29- Oct. 3, 1997.

Parameter	ISS c-Si	Linear Conc.	α-SiGe Thin Film	CuInS2 Thin Film
BOL Power (kW)	1270	948	1154	1050
EPS Mass (MT)				
PV Array	40.0	16.0	7.4	4.8
Array Gimbals	0.0	1.3	0.0	0.0
Batteries	0.2	0.2	0.2	0.2
PMAD	4.3	3.5	4.2	4.0
TCS	0.6	0.4	0.5	0.4
Total	46.1	21.4	12.3	9.4
PV Array Area (m2)	13984	3472	8976	5808
# cells/string	1450	270	340	883
# strings	992	912	9504	2368
DENI Fluence (#/cm2)				
Current	1.0E16	2.2E14	5.9E14	5.9E14
Voltage	2.6E16	3.7E14	1.3E15	1.3E14
Max. Leakage Current (A)	257	1	0	0

Table 1. SEP Stage EPS Sizing Results versus PV Array Technology

Parameter	PV Array Technology	
	α-SiGe	Conc.
EPS Mass (kg)	151	364
PV Array Area (m2)	106	62
Power (kWe)		
1.0 AU	15.5	15.6
5.2 AU*	0.40	0.42
PV Array Temperature (°C)		
1.0 AU	49.1	38.3
5.2 AU	-129.7	-126.2

* - At the beginning of end game

Table 2. Europa Mapper EPS Sizing & Performance Results
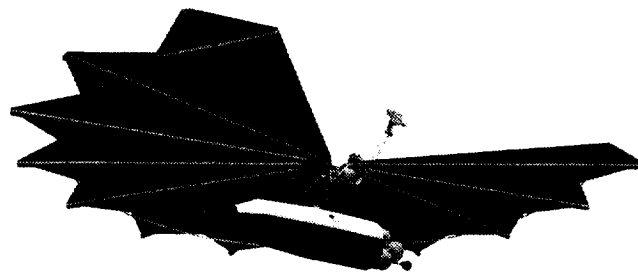
Figure 2. SEP Stage With Payload for Human Mars Mission
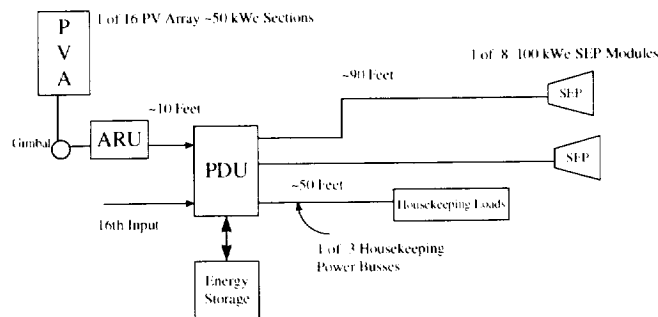
Figure 3. EPS Block Diagram
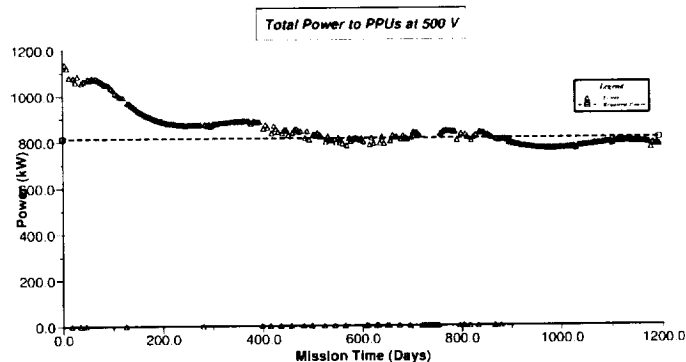
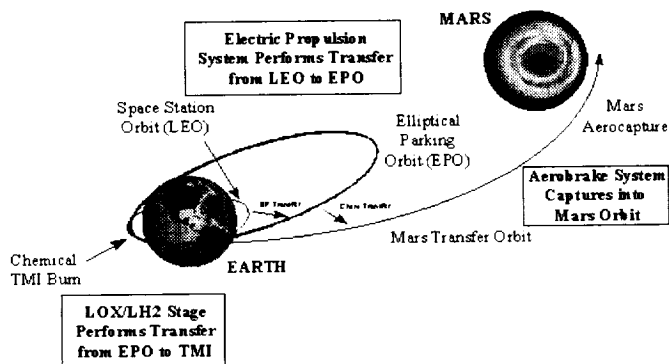
Figure 4. Power To Hall Thrusters

Figure 1. Trans-Mars Injection Using Solar Electric Propulsion and a Cryogenic Stage.
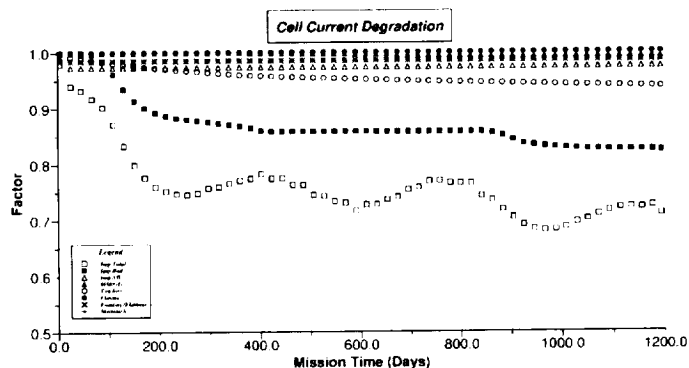

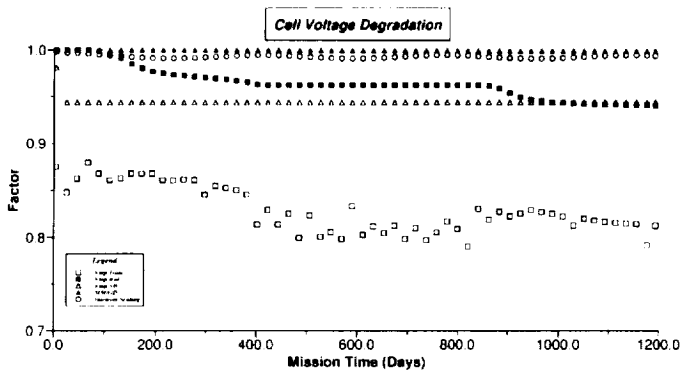Figure 5a. PV Array Degradation (Max. Power Current)

Figure 5b. PV Array Degradation (Max. Power Voltage)
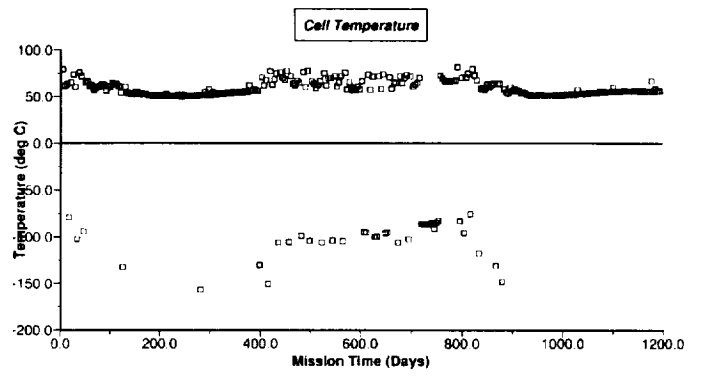

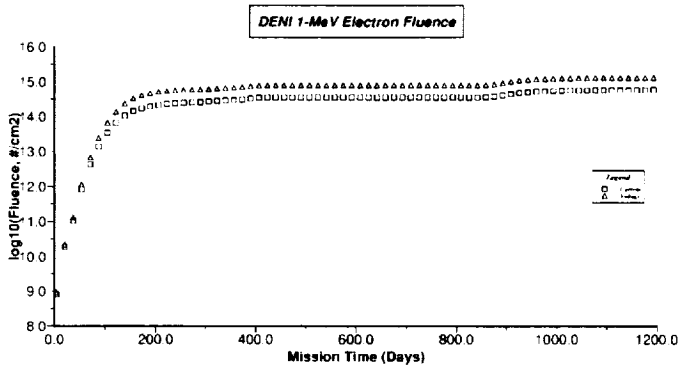Figure 8. PV Array Temperature

Figure 6. DENI Fluence for Thin Film PV Array

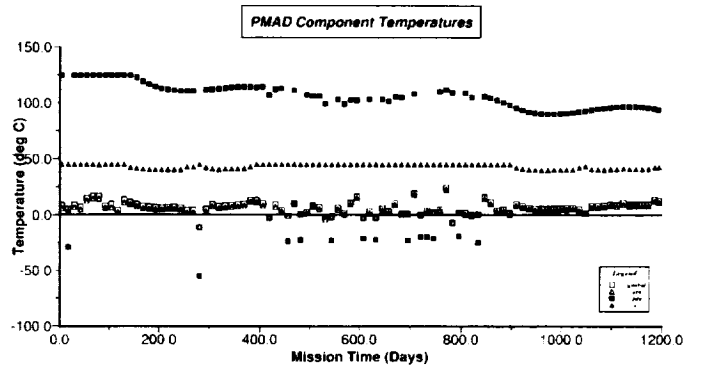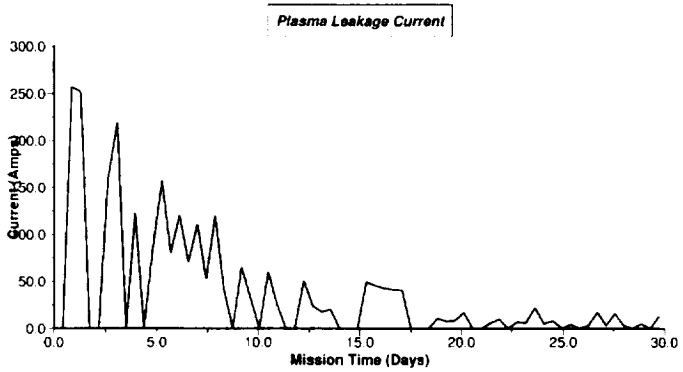Figure 9. PMAD Box Temperatures

Figure 7. Parasitic Plasma Leakage Current for ISS Type
PV Array

REPORT DOCUMENTATION PAGE

Public reporting burden for this collection of information is estimated to average 1 hour per response, including the time for reviewing instructions, searching existing data sources, gathering and maintaining the data needed, and completing and reviewing the collection of information. Send comments regarding this burden estimate or any other aspect of this collection of information, including suggestions for reducing this burden, to Washington Headquarters Services, Directorate for Information Operations and Reports, 1215 Jefferson Davis Highway, Suite 1204, Arlington, VA 22202-4302, and to the Office of Management and Budget, Paperwork Reduction Project (0704-0188), Washington, DC 20503.

1. AGENCY USE ONLY (Leave blank)	2. REPORT DATE	3. REPORT TYPE AND DATES COVERED
	July 1999	Technical Memorandum

4. TITLE AND SUBTITLE

Solar Power System Analyses for Electric Propulsion Missions

5. FUNDING NUMBERS

WU–632–1A–1X–00

6. AUTHOR(S)

Thomas W. Kerslake and Leon P. Gefert

7. PERFORMING ORGANIZATION NAME(S) AND ADDRESS(ES)

National Aeronautics and Space Administration
John H. Glenn Research Center at Lewis Field
Cleveland, Ohio 44135–3191

8. PERFORMING ORGANIZATION REPORT NUMBER

E–11759

9. SPONSORING/MONITORING AGENCY NAME(S) AND ADDRESS(ES)

National Aeronautics and Space Administration
Washington, DC 20546–0001

10. SPONSORING/MONITORING AGENCY REPORT NUMBER

NASA TM—1999-209289
SAE 99–01–2449

11. SUPPLEMENTARY NOTES

12a. DISTRIBUTION/AVAILABILITY STATEMENT

12b. DISTRIBUTION CODE

13. ABSTRACT (Maximum 200 words)

Solar electric propulsion (SEP) mission architectures are applicable to a wide range of NASA missions including human Mars exploration and robotic exploration of the outer planets. In this paper, we discuss the conceptual design and detailed performance analysis of an SEP stage electric power system (EPS). EPS performance, mass and area predictions are compared for several PV array technologies. Based on these studies, an EPS design for a 1-MW class, Human Mars Mission SEP stage was developed with a reasonable mass, 9.4 metric tons, and feasible deployed array area, 5800 m2. An EPS was also designed for the Europa Mapper spacecraft and had a mass of 151 kg and a deployed array area of 106 m2.

14. SUBJECT TERMS

Solar arrays; Electric power; Solar electric propulsion; Performance prediction; Orbit transfer vehicles

15. NUMBER OF PAGES

14

16. PRICE CODE

A03

17. SECURITY CLASSIFICATION OF REPORT	18. SECURITY CLASSIFICATION OF THIS PAGE	19. SECURITY CLASSIFICATION OF ABSTRACT	20. LIMITATION OF ABSTRACT
Unclassified	Unclassified	Unclassified	